

1 **Dynamics of ITCZ width: Ekman processes, non-Ekman processes and**
2 **links to sea-surface temperature**

3 **This work has been submitted to Journal of the Atmospheric
4 Sciences. Copyright in this work may be transferred without
5 further notice.**

6 Michael P. Byrne*

7 *University of St Andrews, Fife, UK and University of Oxford, Oxford, UK*

8 Rhidian Thomas

9 *Imperial College, London, UK*

10 *Corresponding author address: Michael P. Byrne, School of Earth & Environmental Sciences,
11 University of St Andrews, KY16 9AL Fife, United Kingdom
12 E-mail: mpb20@st-andrews.ac.uk

ABSTRACT

13 The dynamical processes controlling the width of the intertropical conver-
14 gence zone (ITCZ) are investigated using idealized simulations. ITCZ width
15 is defined in terms of boundary-layer vertical velocity. The tropical boundary
16 layer is approximately in Ekman balance suggesting that wind stress places
17 a strong constraint on ITCZ width. A scaling based on Ekman balance pre-
18 dicts that ITCZ width is proportional to the wind stress and inversely pro-
19 portional to its meridional gradient. A toy model of an Ekman boundary
20 layer illustrates the effects of wind-stress perturbations on ITCZ width. A
21 westerly wind perturbation widens the ITCZ whereas an easterly perturba-
22 tion narrows the ITCZ. Multiplying the wind stress by a constant factor does
23 not shift the ITCZ edge, but ITCZ width is sensitive to the latitude of maxi-
24 mum wind stress. Scalings based on Ekman balance cannot fully capture the
25 behavior of ITCZ width across simulations, suggesting that non-Ekman dy-
26 namical processes need to be accounted for. An alternative scaling based on
27 the full momentum budget explains variations in ITCZ width and highlights
28 the importance of horizontal and vertical momentum advection. Scalings are
29 also introduced linking ITCZ width to surface temperature. An extension to
30 Lindzen-Nigam theory predicts that ITCZ width scales with the latitude where
31 the Laplacian of SST is zero. The supercriticality theory of Emanuel (1995) is
32 also invoked to show that ITCZ width is dynamically linked to boundary-layer
33 moist entropy gradients. The results establish a dynamical understanding of
34 ITCZ width that can be applied to interpret persistent ITCZ biases in climate
35 models and the response of tropical precipitation to climate change.

36 **1. Introduction**

37 The intertropical convergence zone (ITCZ) is a planetary-scale band of low-level mass conver-
38 gence and intense rainfall (Waliser and Gautier 1993). The ITCZ migrates north and south across
39 the equator in response to seasonal changes in insolation. Given its dominant influence on tropical
40 hydroclimate and importance for societies at low latitudes, the physical mechanisms controlling
41 the ITCZ have received considerable attention (e.g., Philander et al. 1996; Broccoli et al. 2006;
42 Kang et al. 2008; Frierson et al. 2013; Donohoe et al. 2013; Bischoff and Schneider 2014; Byrne
43 and Schneider 2016a). The bulk of ITCZ research has focused on the mechanisms controlling its
44 mean position or latitude, and these mechanisms are now well understood at least in the zonal-
45 mean context (see reviews by Chiang and Friedman 2012; Schneider et al. 2014; Donohoe and
46 Voigt 2017; Kang et al. 2018). By comparison, the processes determining the width of the ITCZ
47 are relatively under-studied despite its importance for regional and global climate. Recent work
48 has shown that ITCZ width influences global precipitation and top-of-atmosphere energy balance
49 (Su et al. 2017; Byrne and Schneider 2018) and is dynamically linked to the poleward extent of the
50 Hadley cell and the latitudes of the storm tracks (Watt-Meyer and Frierson 2019). Furthermore,
51 changes in ITCZ width in response to radiative forcing are strongly anti-correlated with changes
52 in ITCZ strength (Byrne et al. 2018), suggesting that a better understanding of the processes con-
53 trolling ITCZ width could help constrain ITCZ strength and tropical rainfall intensity.

54 We currently lack a closed theory for ITCZ width and its response to climate perturbations. In
55 recent years, however, progress has been made in understanding how different processes affect
56 ITCZ width. A theory derived from atmospheric mass and moist static energy budgets shows
57 how the ITCZ narrows or widens in response to changes in gross moist stability, cloud radiative
58 effects, energy/moisture advection and moisture transport by transient eddies (Byrne and Schnei-

59 der 2016a); other studies also identified that these processes can affect ITCZ width (Bretherton
60 and Sobel 2002; Sobel 2003; Chou and Neelin 2004; Sobel and Neelin 2006; Chou et al. 2009;
61 Harrop and Hartmann 2016; Popp and Silvers 2017; Dixit et al. 2018; Emanuel 2019). This en-
62 energetic theory has been used to quantify the processes contributing to projected narrowing of the
63 ITCZ in coupled climate models (Byrne and Schneider 2016b) and could potentially be applied to
64 understand the observed ITCZ narrowing over recent decades (Wodzicki and Rapp 2016).

65 Despite these recent advances in our mechanistic understanding of ITCZ width, there are oppor-
66 tunities for further progress by considering the dynamics of the atmospheric boundary layer. The
67 boundary-layer momentum budget has been successfully invoked to explain the spatial distribu-
68 tion of tropical low-level convergence and precipitation (Lindzen and Nigam 1987; Waliser and
69 Somerville 1994; Tomas et al. 1999; Stevens et al. 2002; Sobel 2007; Gonzalez et al. 2016) but
70 has not been applied specifically to the problem of ITCZ width. There has been a long-standing
71 debate in the atmospheric dynamics community regarding whether tropical convergence is driven
72 by boundary-layer dynamics or by thermodynamic processes higher in the atmosphere such as
73 latent-heat release [see section 2 of Sobel and Neelin (2006) for a summary of these compet-
74 ing arguments]. Now there is a developing consensus that low-level convergence — and hence
75 ITCZ width — is primarily controlled by surface pressure gradients and boundary-layer dynamics
76 (Lindzen and Nigam 1987; Sobel and Neelin 2006; Back and Bretherton 2009). It is therefore
77 important to develop an understanding of ITCZ width from a dynamics perspective to comple-
78 ment the recent studies based on energetics and thermodynamics (Chou et al. 2009; Byrne and
79 Schneider 2016a; Harrop and Hartmann 2016; Popp and Silvers 2017; Dixit et al. 2018).

80 Here we use the boundary-layer zonal momentum budget together with idealized simulations
81 to investigate the dynamics of ITCZ width. In particular, we examine the momentum budget
82 near the ITCZ edge, assess the dominant terms, and quantify the processes controlling low-level

83 convergence and vertical velocity in that region. We also derive a range of scalings for ITCZ
84 width and assess the importance of Ekman vs non-Ekman processes. Finally, we link ITCZ width
85 to sea-surface temperature (SST) and boundary-layer moist entropy using simple extensions to the
86 theories of Lindzen and Nigam (1987) and Emanuel (1995).

87 **2. Simulations**

88 *a. Idealized GCM*

89 We perform simulations using the idealized, grey-radiation GCM of O’Gorman and Schneider
90 (2008) based on the model developed by Frierson et al. (2006) and Frierson (2007). Insolation
91 is set to an annual-mean profile and the longwave optical thickness is specified as a function
92 of latitude and pressure. All the idealized simulations discussed here are run in an aquaplanet
93 configuration with a mixed layer of depth 1m and no horizontal energy transports (zero q-fluxes).
94 The aquaplanet configuration has no inter-hemispheric asymmetries in statistical steady state and
95 consequently the ITCZ is centered on the equator. The model has a horizontal spectral resolution
96 of T127, 20 vertical σ -levels and an integration timestep of 150 seconds. Simulations are spun
97 up for 700 days with averages taken over the subsequent 1000 days. See Byrne and Schneider
98 (2016a) for an extended description of the model setup.

99 In the set of simulations analyzed here, the longwave optical thickness is varied so as to mimic
100 changes in greenhouse-gas concentrations. We analyze a suite of 11 simulations: The longwave
101 optical thickness for each simulation is based on a reference profile that has been re-scaled by
102 different factors α^1 .

¹For the idealized-GCM simulations we re-scale the longwave optical thickness of a reference simulation by the following factors: $\alpha =$
0.4, 0.5, 0.7, 0.8, 1.0, 1.2, 1.5, 1.8, 2.0, 2.5, 3.0.

103 *b. CMIP5 models*

104 We also examine ITCZ width in three fixed-SST aquaplanet simulations from the Coupled
105 Model Intercomparison Project Phase 5 (CMIP5) (Taylor et al. 2012): *aquaControl*, *aqua4K* and
106 *aqua4xCO2*. Simulations from the IPSL-CM5A-LR, CNRM-CM5, IPSL-CM5B-LR, FGOALS-
107 g2, MIROC5, HadGEM2-A, MPI-ESM-MR, MRI-CGCM3, and MPI-ESM-LR climate models
108 are analyzed.

109 **3. Boundary-layer dynamics near the ITCZ edge**

110 *a. Definition of ITCZ width*

111 We define ITCZ width as the degrees latitude between the northern and southern ITCZ edges.
112 The edges of the ITCZ are defined as the latitudes closest to the equator (north and south) at
113 which the time-mean vertical velocity at the boundary-layer top is zero. In the idealized-GCM
114 simulations we specify the boundary-layer top as the $\sigma = 0.8$ level. This is similar to the definition
115 of Byrne and Schneider (2016a) but in their analysis the mid-tropospheric mass streamfunction is
116 used to define the ITCZ edges. We choose to focus on the boundary-layer ITCZ width because it
117 is more directly connected to the boundary-layer momentum budget, which is the tool used here to
118 investigate the ITCZ. In addition, rainfall is driven by low-level convergence and vertical velocity
119 at the boundary-layer top, and so a boundary-layer definition of ITCZ width is expected to be more
120 relevant for rainfall and the hydrological cycle. Although we will mostly focus on the boundary-
121 layer definition of ITCZ width, in Section 4 we discuss how ITCZ widths based on boundary-layer
122 vs mid-tropospheric definitions do not always behave similarly as climate in varied, and that the
123 utility of dynamical scalings for ITCZ width can depend on the definition used.

124 *b. ITCZ width vs global-mean SST in idealized-GCM simulations*

125 The average ITCZ width across the set of simulations over which longwave optical thickness
 126 is varied is 9.6° latitude; the width varies by 4° as the global-mean SST is increased from 272 K
 127 to 306 K (Figure 1a). ITCZ width does not change monotonically with global warming in these
 128 idealized simulations, rather the ITCZ widens with warming in cooler climate and narrows with
 129 warming in hotter climates. Here we use boundary-layer dynamics to analyze these variations of
 130 ITCZ width with global-mean SST.

131 *c. Zonal momentum budget*

132 We start with the steady-state zonally-averaged zonal momentum equation [see Peixóto and Oort
 133 (1984)]:

$$fv = -F_x - \frac{\tan \phi}{a} uv + \frac{v}{a} \frac{\partial u}{\partial \phi} + \omega \frac{\partial u}{\partial p}, \quad (1)$$

134 where $f = 2\Omega \sin \phi$ is the Coriolis parameter, F_x is the zonal component of the frictional force, a is
 135 Earth's radius, ϕ is latitude in radians, ω is the vertical (pressure) velocity, and the other symbols
 136 have their usual meanings. Taking the mass-weighted vertical average over the boundary layer,
 137 equation (1) becomes:

$$\underbrace{f[v]}_{\text{Coriolis}} = \overbrace{-(g/\Delta p)\tau_{x,\text{sfc}}}^{\text{frictional}} - \underbrace{\frac{\tan \phi}{a}[uv]}_{\text{metric}} + \overbrace{\left[\frac{v}{a} \frac{\partial u}{\partial \phi}\right]}^{\text{horiz. adv.}} + \underbrace{\left[\omega \frac{\partial u}{\partial p}\right]}_{\text{vert. adv.}}, \quad (2)$$

138 where $[\cdot]$ denotes a mass-weighted vertical average over the boundary layer, g is the acceleration
 139 due to gravity, $\Delta p = p_s - p_{\text{BL}}$ is the pressure difference between the surface and the boundary-
 140 layer top, and $\tau_{x,\text{sfc}}$ is the zonal component of the vertical turbulent stress (which we will call
 141 the zonal wind stress). The various forces have been labeled: Coriolis, frictional, metric and

142 horizontal/vertical advection of relative momentum. In deriving (2), we have assumed that the
143 turbulent stress vanishes at the boundary-layer top.

144 In the reference idealized-GCM simulation ($\alpha = 1.0$), the Coriolis and frictional terms dominate
145 the zonal momentum budget in the vicinity of the ITCZ edge (Figures 1b and 2a). The vertical
146 and horizontal momentum advection terms have similar magnitudes but both are substantially
147 smaller than the Coriolis and frictional terms; the metric term is negligible (Figure 2a) and will
148 not be discussed further. It is common to assume Ekman balance in the tropical atmospheric
149 boundary layer, i.e. a balance between Coriolis and frictional forces (e.g., Lindzen and Nigam
150 1987; Emanuel 1995; Held 2001). This force balance holds approximately at the ITCZ edge
151 across the wide range of climates simulated by the idealized GCM (Figure 1b), which suggests
152 that Ekman balance is a natural starting point for understanding the dynamics of ITCZ width. A
153 recent study found that Ekman balance breaks down near the ITCZ, at least in a dry equatorial β -
154 plane model of the tropical boundary layer, because the horizontal-advection term becomes large
155 (Gonzalez et al. 2016). In our idealized-GCM simulations we note that the vertical- and horizontal-
156 advection terms become relatively more important at the ITCZ edge in warmer climates as the
157 magnitudes of the Coriolis and frictional terms decrease (Figure 1b). However, the zeroth-order
158 balance is between Coriolis and frictional accelerations across all idealized-GCM simulations.

159 In the boundary-layer momentum budget the frictional force provides an eastward acceleration
160 to the zonal wind at the ITCZ edge because the tropical surface winds are easterly (Figure 2b);
161 there is a transfer of zonal momentum from the surface to the overlying atmosphere. This eastward
162 acceleration is largely balanced by westward acceleration associated with equatorward advection
163 of air with relatively low planetary angular momentum by the surface branch of the Hadley cell
164 (the Coriolis term). For all except the coldest two simulations (Figure 1b), both the vertical- and
165 horizontal-advection terms provide a westward acceleration to the boundary-layer zonal wind at

166 the ITCZ edge by advecting low-angular momentum air. The horizontal-advection term acceler-
 167 ates the easterly zonal wind at the ITCZ edge provided the maximum in tropical surface easterlies
 168 is poleward of the ITCZ edge, as is the case in the reference simulation (Figure 2b). Equivalently,
 169 if the latitude of zero surface relative vorticity (where $\partial u_{\text{sfc}}/\partial\phi = 0$) lies poleward of the ITCZ
 170 edge, the horizontal advection term will accelerate the easterly zonal flow there. For the vertical-
 171 advection term, if the latitude at which the flow is non-divergent (i.e. where $\partial\omega/\partial p = 0$) did not
 172 vary with height, the vertical advection term in (2) would be identically zero at the ITCZ edge.
 173 However, the latitude of non-divergence does vary with height in the idealized-GCM simulations
 174 (not shown). Consequently the vertical advection term in the zonal momentum budget is non-zero
 175 and accelerates the easterly zonal wind for the majority of simulations (Figure 1b).

176 **4. Scalings for ITCZ width based on Ekman balance**

177 We have demonstrated that the boundary layer at the ITCZ edge is approximately in Ekman
 178 balance in the idealized GCM (Figure 1b). We now use Ekman balance to derive simple dynamical
 179 scalings for ITCZ width and apply these scalings to the idealized-GCM and CMIP5 simulations.

180 *a. Relationship between ITCZ width, wind stress and vorticity*

181 Perhaps the simplest estimate for the latitude of the ITCZ edge (and ITCZ width) is obtained
 182 by assuming Ekman balance in the atmospheric boundary layer and taking the wind stress to be
 183 linearly proportional to the surface wind (e.g., Held and Hou 1980):

$$f[v] = C u_{\text{sfc}}, \quad (3)$$

184 where C is a constant drag coefficient. Combining (3) with the zonally-averaged mass continuity
 185 equation in pressure coordinates², assuming zero vertical velocity at the surface, and for now ne-
 186 glecting meridional variations in the Coriolis parameter, it is straightforward to show that vertical
 187 velocity at the top of the boundary layer (ω_{BL}) is proportional to the surface relative vorticity:
 188 $\omega_{\text{BL}} \propto \partial u_{\text{sfc}} / \partial \phi$. This relationship suggests that the ITCZ-edge latitude, where $\omega_{\text{BL}} = 0$ by defi-
 189 nition, scales with the latitude where $\partial u_{\text{sfc}} / \partial \phi = 0$ and the surface flow transitions from cyclonic
 190 to anti-cyclonic relative vorticity.

191 Testing this simple prediction in the idealized GCM, we find that the latitude of zero relative vor-
 192 ticity does not scale monotonically with the ITCZ edge defined in terms of boundary-layer vertical
 193 velocity (black circles in Figure 3). This implies, perhaps not surprisingly, that frictional Ekman
 194 convergence alone — where we have also neglected the component due to meridional gradients
 195 in the reciprocal of the Coriolis parameter — cannot capture the behavior of ITCZ width over
 196 the full range of idealized-GCM simulations. Interestingly, there is a strong correlation between
 197 the latitude of zero relative vorticity and the ITCZ edge defined in terms of the mid-tropospheric
 198 streamfunction (red circles in Figure 3) though the latitude of zero relative vorticity tends to un-
 199 derestimate the ITCZ width. From a dynamics perspective, the variation of the ITCZ edge with
 200 height and the contrasting scaling relationships between different ITCZ-width definitions (Figure
 201 3) is likely due to terms in the zonal momentum budget being more or less influential at different
 202 levels in the atmosphere — this is a question to be investigated in future work. What is clear is that
 203 surface relative vorticity is closely tied to ITCZ width in the mid-troposphere but the connection
 204 to ITCZ width at the top of the boundary layer is more complex.

205 Related to this simple estimate for the ITCZ-edge latitude, Tomas and Webster (1997) argue that
 206 the barrier between boundary-layer convergence and divergence in the tropics (which is the ITCZ

²The steady-state continuity equation written in pressure coordinates is: $\frac{1}{a \cos \phi} \frac{\partial}{\partial \phi} (v \cos \phi) + \frac{\partial \omega}{\partial p} = 0$.

207 edge by our boundary-layer definition) coincides with the zero contour of the vertical component
208 of *absolute* vorticity, where absolute vorticity in the zonal mean is $\eta = f - \frac{1}{a} \frac{\partial u_{\text{sfc}}}{\partial \phi}$. If the product
209 of the Coriolis parameter and absolute vorticity is negative ($f\eta < 0$) this implies that the flow is
210 inertially unstable; Tomas and Webster (1997) find evidence of such unstable regions close to the
211 equator and find that they are associated with cross-equatorial advection of absolute vorticity by
212 large pressure gradients at the equator. In our idealized-GCM simulations, however, there are no
213 inter-hemispheric asymmetries and so there is no time-mean pressure gradient at the equator and
214 the zero contour of absolute vorticity lies at the equator. Consequently, the Tomas and Webster
215 (1997) theory cannot explain the off-equatorial ITCZ edges in our simulations.

216 A more complete description of Ekman balance that includes the GCM-simulated wind stress
217 $\tau_{x,\text{sfc}}$ but still neglects the meridional gradient of $1/f$, suggests that the ITCZ edge should scale
218 with the latitude where the easterly wind stress maximizes, i.e. where $\partial \tau_{x,\text{sfc}} / \partial \phi = 0$. The es-
219 timates of the ITCZ edge based on where wind stress maximizes are very similar to those based
220 on the latitude of zero relative vorticity (Figure 3). This agreement indicates that, at least for
221 the idealized-GCM simulations, the simplifying assumptions of linear drag and a constant drag
222 coefficient are reasonable when investigating ITCZ width.

223 Figure 3 demonstrates that the surface wind stress alone cannot fully capture the dynamics of
224 boundary-layer ITCZ width. Before considering how other terms in the momentum budget affect
225 ITCZ width (specifically momentum advection), we first explore in more depth the implications of
226 perfect Ekman balance for ITCZ width. In particular, we derive additional Ekman scalings for the
227 ITCZ-edge latitude and perturbations to this latitude that account for meridional structure in the
228 Coriolis parameter and give conceptual insights into the coupling between wind stress and ITCZ
229 width.

230 *b. An Ekman scaling for ITCZ width*

231 Further insights into the relationship between ITCZ width and wind stress can be obtained by
232 rearranging (8). In particular, making the small-angle approximation so that $f = 2\Omega \sin \phi \approx 2\Omega \phi$
233 (valid close to the equator), ignoring the meridional gradients of $\cos \phi$ and Δp , and noting that
234 $\omega_{\text{BL}}(\phi_{\text{ITCZ}}) = 0$ by definition, we obtain an expression for the ITCZ-edge latitude (ϕ_{ITCZ}) assum-
235 ing Ekman balance:

$$\phi_{\text{ITCZ}}^{\text{ekman}} = \tau_{x,\text{sfc}}(\phi_{\text{ITCZ}}) / \left. \frac{\partial \tau_{x,\text{sfc}}}{\partial \phi} \right|_{\phi=\phi_{\text{ITCZ}}}, \quad (4)$$

236 where all quantities on the right-hand side are evaluated at the ITCZ edge. The diagnostic scaling
237 (4) suggests that the latitude of the ITCZ edge (in radians) is directly proportional to the wind
238 stress and inversely proportional to the meridional gradient of the wind stress. Figures 4 and 5
239 show estimates of the ITCZ-edge latitude using (4) in the idealized-GCM and CMIP5 simulations.
240 Clearly Ekman dynamics as encapsulated in (4) captures some of the behavior of ITCZ width
241 across the idealized ($r = 0.81$) and CMIP5 simulations ($r = 0.83$) but the estimates depart from
242 the simulated ITCZ edges. This discrepancy hints at the importance of other processes — we
243 investigate these processes in Sections 5 and 6. Nevertheless, the strong correlations in Figures
244 4 and 5 highlight a robust link between ITCZ width and Ekman balance. Before examining non-
245 Ekman processes, we first use a toy model of the tropical boundary layer to further elucidate the
246 implications of Ekman balance for ITCZ width.

247 *c. Impact of wind-stress perturbations on ITCZ width: investigations with a toy model*

248 The diagnostic scaling (4) shows how, assuming Ekman balance, the ITCZ-edge latitude relates
249 to the magnitude and gradient of the zonal wind stress. But how do *perturbations* in wind stress,
250 for example due to changes in windspeed or surface roughness, impact ITCZ width? To develop

251 intuition for how ITCZ width is controlled by the wind stress, consider a stylized, reference zonal
 252 wind stress profile: $\tau_{\text{ref}}(\phi) = v_{\text{max}} \times (f\Delta p/g) \sin 9\phi$ (Figure 6a). This wind stress is defined to
 253 be in Ekman balance with a reference boundary-layer meridional wind $v(\phi) = v_{\text{max}} \sin 9\phi$ (Figure
 254 6b). We specify $v_{\text{max}} = -5$ m/s and $\Delta p = 100$ hPa. For these reference profiles, the magnitude of
 255 the meridional wind maximizes at 10°N ; the ITCZ-edge latitude is shifted marginally equatorward
 256 (9.9°N) because of the $\cos \phi$ weighting when calculating convergence and vertical velocity (Figure
 257 6c). The maximum wind stress is on the poleward side of the ITCZ edge at 12.9°N (Figure 6a) as is
 258 also the case in the idealized-GCM simulations (Figure 3). This displacement between the latitudes
 259 of maximum wind stress and ITCZ edge in the toy model is caused by meridional gradients in the
 260 reciprocal of the Coriolis parameter.

261 We now perturb the reference stress profile in three ways and assess how these perturbations
 262 affect the ITCZ width:

- 263 1. *Add/subtract a constant stress:* Adding a constant westerly wind stress of 0.03 N/m^2 at all
 264 latitudes shifts the ITCZ edge poleward relative to its reference position by 0.8° . Adding a
 265 constant easterly wind stress of 0.03 N/m^2 shifts the ITCZ edge equatorward by 1.3° (Figure
 266 6a,b,c).
- 267 2. *Multiply/divide stress by a factor of 2:* Multiplying or dividing the wind stress by 2 does not
 268 shift the ITCZ edge (Figure 6d,e,f), despite the imposed changes in stress being substantially
 269 larger than in the previous case where we added a constant stress.
- 270 3. *Shift latitude of maximum stress:* Manipulating the reference stress profile so as to shift the
 271 latitude of maximum stress equatorward and poleward has a large, amplified effect on the
 272 ITCZ-edge latitude (Figure 6g,h,i). Specifically, shifting the stress maximum equatorward by

1.1° causes an ITCZ shift of 3.4°; shifting the stress maximum poleward by 1.3° shifts the ITCZ edge poleward by 2.7°.

The Ekman scaling (4) we derived above is diagnostic but can be extended to provide simple explanations for the contrasting responses of ITCZ width to the imposed changes in wind stress described above. First define a function $\gamma(\phi) = \phi \frac{\partial \tau_{x,\text{sfc}}}{\partial \phi} - \tau_{x,\text{sfc}}$ which, according to (4), is zero at the ITCZ edge under the assumption of Ekman balance. We are interested in how ITCZ width responds to an arbitrary wind-stress perturbation. Using a first-order Taylor expansion of the perturbed function $\gamma(\phi)$ [denoted $\gamma'(\phi)$] about the reference ITCZ-edge latitude, we can approximate the change in ϕ_{ITCZ} as:

$$\delta \phi_{\text{ITCZ}} \approx -\gamma'(\phi_{\text{ITCZ}}) / \left. \frac{\partial \gamma}{\partial \phi} \right|_{\phi_{\text{ITCZ}}}, \quad (5)$$

where ϕ_{ITCZ} is the reference ITCZ-edge latitude.

Now we use (5) to interpret the ITCZ-edge shifts in Figure 6. Adding a constant wind stress $\delta \tau$ changes the magnitude of $\tau_{x,\text{sfc}}$ but not its meridional gradient, and so $\gamma'(\phi_{\text{ITCZ}}) = -\delta \tau$ and $\left. \frac{\partial \gamma}{\partial \phi} \right|_{\phi_{\text{ITCZ}}} = \left. \phi_{\text{ITCZ}} \frac{\partial^2 \tau_{x,\text{sfc}}}{\partial \phi^2} \right|_{\phi_{\text{ITCZ}}}$, resulting in an expression for the change in ITCZ width in response to a constant wind-stress perturbation:

$$\delta \phi_{\text{ITCZ}} \approx \frac{1}{\phi_{\text{ITCZ}}} \left. \frac{\delta \tau}{\partial^2 \tau_{x,\text{sfc}} / \partial \phi^2} \right|_{\phi_{\text{ITCZ}}} \quad \text{for } \tau'_{x,\text{sfc}} = \tau_{\text{ref}} + \delta \tau, \text{ where } \delta \tau \text{ is a constant.} \quad (6)$$

The expression (6) reveals that the ITCZ-edge shift is directly proportional to the perturbation stress $\delta \tau$, and inversely proportional to the curvature of the reference $\tau_{x,\text{sfc}}$ profile. For the wind-stress profiles considered in this toy model (Figure 6a,d,g), the curvature term is positive in the vicinity of the ITCZ edge ($\partial^2 \tau_{x,\text{sfc}} / \partial \phi^2 > 0$). Consequently, adding a westerly stress (e.g. through weakened surface easterlies) widens the ITCZ whereas adding an easterly stress narrows the ITCZ

292 (Figure 6c). This scaling of ITCZ width with wind stress is supported by the idealized-GCM
 293 simulations (Figure 7). The asymmetry in the magnitudes of ITCZ-width responses to adding a
 294 westerly vs an easterly stress perturbation (Figure 6a,b,c) is not captured by the first-order Taylor
 295 expansion used to derive (6), but could be investigated with a higher-order expansion.

296 We can also use (5) to understand how scaling the wind stress by a constant factor μ affects
 297 the ITCZ width. We assume again for simplicity that the atmospheric boundary layer is in Ekman
 298 balance. For this wind-stress perturbation it is straightforward to show that $\gamma'(\phi_{\text{ITCZ}}) = 0$ and thus
 299 for non-zero curvature in $\tau_{x,\text{sfc}}$ there is no change in ITCZ width (see Figure 6f):

$$\delta\phi_{\text{ITCZ}} = 0 \text{ for } \tau'_{x,\text{sfc}} = \mu\tau_{\text{ref}}. \quad (7)$$

300 Simple analytical expressions for changes in ITCZ width due to shifting the latitude of maximum
 301 wind stress (Figure 6g,h,i) are not as straightforward as for the previous two cases though could be
 302 derived using (5). What is clear is that subtle shifts in the latitude of maximum stress can lead to
 303 amplified shifts in ITCZ edge and that, perhaps intuitively, the ITCZ narrows when the maximum
 304 in wind stress moves towards the equator and widens when it moves poleward.

305 **5. Boundary-layer convergence: Ekman vs non-Ekman processes**

306 As discussed, Ekman dynamics cannot fully capture the behavior for ITCZ width across all
 307 simulations and additional processes need to be considered. ITCZ width is defined as a function
 308 of vertical velocity at the top of the boundary layer: The influences of Ekman vs non-Ekman
 309 processes on ITCZ width can be decomposed by assessing their respective contributions to ω_{BL}
 310 near the ITCZ edge. To perform this decomposition, we first convert the zonal momentum budget
 311 (2) into an equation for boundary-layer mass convergence and vertical velocity.

312 Neglecting the metric term in (2), dividing across by the Coriolis parameter, taking the derivative
 313 with respect to latitude, combining with the continuity equation and again assuming $\omega = 0$ at the
 314 surface, we obtain the following expression for vertical velocity at the boundary-layer top:

$$\omega_{\text{BL}} = \underbrace{-\frac{g}{a \cos \phi} \frac{\partial}{\partial \phi} \left(\frac{\tau_{x,\text{sfc}}}{f} \cos \phi \right)}_{\omega_{\text{ekman}}} + \overbrace{\frac{\Delta p}{a \cos \phi} \frac{\partial}{\partial \phi} \left(\frac{\cos \phi}{f} \left[\omega \frac{\partial u}{\partial p} \right] \right)}^{\omega_{\text{vert}}} + \underbrace{\frac{\Delta p}{a \cos \phi} \frac{\partial}{\partial \phi} \left(\frac{\cos \phi}{f} \left[\frac{v}{a} \frac{\partial u}{\partial \phi} \right] \right)}_{\omega_{\text{horiz}}}. \quad (8)$$

315 The total vertical velocity is split into three components: A component associated with frictional
 316 Ekman convergence (ω_{ekman}) and components related to vertical and horizontal advection of rela-
 317 tive momentum (ω_{vert} and ω_{horiz} , respectively). The components of vertical velocity in the vicinity
 318 of the ITCZ edge are plotted as a function of latitude for the reference simulation in Figure 8.
 319 The sum of the three components is approximately equal to the simulated vertical velocity; the
 320 small differences are due to the metric and residual terms in the zonal momentum budget being
 321 neglected.

322 Although the Coriolis and frictional terms approximately balance one another in the zonal mo-
 323 mentum budget (Figure 1b), Ekman balance is insufficient for accurately estimating vertical ve-
 324 locity close to and within the ITCZ (Figure 8). It is therefore clear why the latitude of the ITCZ
 325 edge cannot be fully understood through Ekman dynamics alone. The vertical and horizontal
 326 advection terms have a relatively weak influence on the zonal momentum budget near the ITCZ
 327 edge (Figure 2a), but it is the meridional gradient of $1/f$ times these advection terms which de-
 328 termines convergence [see equation (8)]. The advection components of the vertical velocity are
 329 non-negligible at the ITCZ edge where they contribute to low-level convergence and ascent (Figure
 330 8). Interestingly, the vertical and horizontal advection terms in the zonal momentum budget at the
 331 ITCZ edge are strongly correlated with one another across the idealized-GCM simulations (Fig-

332 ure 9). The importance of vertical advection of momentum between the boundary layer and free
333 troposphere for determining tropical surface winds has been discussed previously (Stevens et al.
334 2002; Back and Bretherton 2009) so it is not surprising that this process affects ITCZ width. The
335 horizontal-advection component ω_{horiz} is comparable to the vertical-advection component ω_{vert}
336 across the idealized-GCM simulations (Figure 10). This term in the zonal momentum budget is
337 often neglected in studies of tropical dynamics (e.g., Lindzen and Nigam 1987) but its importance
338 for shaping tropical convergence has been highlighted previously (Holton 1975; Gonzalez et al.
339 2016). There is Ekman-driven descent at the ITCZ edge in the reference simulation (Figure 8) and
340 across all the idealized-GCM simulations (Figure 10). In the majority of simulations the vertical
341 and horizontal advection terms drive convergence and ascent at the ITCZ edge (Figures 8 and 10)
342 and thus tend to widen the ITCZ relative to a hypothetical boundary layer in perfect Ekman bal-
343 ance. Figure 8 shows that vertical and horizontal momentum advection are crucial for the spatial
344 distribution of convergence and rainfall in the tropics — we will return to the influence of these
345 advection processes on ITCZ width in the next section.

346 *a. Influence of meridional gradients in the Coriolis parameter on ITCZ width*

347 Vertical velocity is driven by components associated with meridional gradients in (i) zonal wind
348 stress and momentum advection and (ii) the reciprocal of the Coriolis parameter (8). It is inter-
349 esting to compare these components: Both are large near the ITCZ (compare the solid and dotted
350 black lines in Figure 8), indicating that ITCZ width is controlled by a delicate balance between
351 the two terms. Meridional structure in the reciprocal of the Coriolis parameter is of zeroth-order
352 importance for ITCZ width; the strong gradient in this function close to the equator drives descent
353 and therefore acts to narrow the ITCZ (Figure 8). The influence of the Coriolis parameter on
354 boundary-layer convergence decays rapidly ($\sim 1/\tan\phi$) moving poleward away from the ITCZ.

355 6. Scaling for ITCZ width based on the full momentum budget

356 The magnitude and pattern of zonal wind stress, via its influence on frictional Ekman conver-
 357 gence, is a strong constraint on ITCZ width (Figures 4, 5 6 and 7). However, in the previous
 358 section we demonstrated that ITCZ width is controlled by convergence driven by wind stress and
 359 horizontal/vertical advection of momentum. Below we introduce a “full” dynamical scaling to
 360 quantitatively investigate these competing physical controls on ITCZ width.

361 It is difficult to cleanly assess the roles of Ekman vs non-Ekman processes in determining the
 362 ITCZ width by examining the components of vertical velocity (8). This is because the Ekman com-
 363 ponent does not pass through zero close to the equator in the idealized GCM and so an “Ekman-
 364 only ITCZ width” is not defined. To quantitatively compare the effects of Ekman vs non-Ekman
 365 processes on ITCZ width, we instead derive an extended version of the analytical scaling (4) for
 366 the ITCZ-edge latitude that includes horizontal and vertical advection of momentum:

$$\phi_{\text{ITCZ}}^{\text{full}} = \frac{-(g/\Delta p)\tau_{x,\text{sfc}} + \left[\omega \frac{\partial u}{\partial p}\right] + \left[\frac{v}{a} \frac{\partial u}{\partial \phi}\right]}{-(g/\Delta p)\frac{\partial \tau_{x,\text{sfc}}}{\partial \phi} + \frac{\partial}{\partial \phi} \left[\omega \frac{\partial u}{\partial p}\right] + \frac{\partial}{\partial \phi} \left[\frac{v}{a} \frac{\partial u}{\partial \phi}\right]} \Bigg|_{\phi=\phi_{\text{ITCZ}}}, \quad (9)$$

367 where all quantities on the right-hand side are evaluated at the ITCZ edge. This “full” dynamical
 368 scaling (9) captures the ITCZ-edge latitude across the full range of idealized-GCM simulations
 369 with a correlation coefficient of $r = 0.96$ (Figure 4) and does reasonably well at capturing the
 370 behavior in more complex CMIP5 simulations ($r = 0.81$; Figure 5). For the idealized-GCM sim-
 371 ulations, comparing the black and red circles in Figure 4 we find that neglecting the momentum
 372 advection terms leads to an error in estimating the ITCZ-edge latitude that is substantial (ap-
 373 proximately 2° latitude) relative to the ITCZ width itself. Clearly momentum advection must be
 374 accounted for in any quantitative theory of ITCZ width. The role of momentum transport by tran-
 375 sient eddies in controlling ITCZ width is illustrated by comparing the blue and black circles in

376 Figure 4. Neglecting vertical and horizontal momentum advection by transient eddies gives errors
377 of approximately 1° in estimates of the ITCZ-edge latitude. This non-negligible influence of tran-
378 sient eddies on ITCZ width is consistent with Byrne and Schneider (2016a,b) who found, using an
379 energetic framework, that transient eddies are a key process controlling ITCZ width.

380 **7. Relationships between ITCZ width and surface temperature, moist entropy**

381 Up to this point we have studied ITCZ width in terms of dynamical quantities, specifically wind
382 stress and momentum advection. It is also useful [and somewhat traditional in the field of tropical
383 atmospheric dynamics (Sobel 2007)] to construct theories connecting the circulation to surface
384 thermodynamic quantities such as SST; below we propose two such theories for ITCZ width.

385 *a. Lindzen-Nigam theory*

386 Lindzen and Nigam (1987) argued that tropical surface winds and convergence are closely con-
387 trolled by the SST distribution via its influence on boundary-layer pressure gradients. In order
388 to make the problem more tractable and link surface winds directly to SST, Lindzen and Nigam
389 (1987) neglected horizontal and vertical momentum advection and assumed that pressure gradi-
390 ents vanish above the boundary layer. Despite the validity of these assumptions being challenged
391 (e.g., Battisti et al. 1999), observations suggest that surface convergence in the tropics is largely
392 driven by pressure gradients within (rather than above) the boundary layer (Back and Bretherton
393 2009). This is a strong indication that SST gradients are dynamically tied to ITCZ width.

394 To make our discussion of the link between ITCZ width and SST more concrete, consider simpli-
395 fied forms of the zonal (10) and meridional (11) momentum equations in Ekman balance following
396 Lindzen and Nigam (1987):

$$f[v] = C[u] \quad (10)$$

$$f[u] = - \left[\frac{1}{\rho a} \frac{\partial p}{\partial \phi} \right] - C[v]. \quad (11)$$

397 In equations (10) and (11) we have assumed for simplicity that the drag coefficient C is the same
 398 for zonal and meridional winds, and have formulated the frictional force in terms of the boundary-
 399 layer average winds. Combining the zonal and meridional momentum equations we obtain an
 400 expression for the meridional wind:

$$[v] = - \frac{C}{f^2 + C^2} \left[\frac{1}{\rho a} \frac{\partial p}{\partial \phi} \right]. \quad (12)$$

401 Ignoring pressure gradients above the boundary layer (which are typically taken to be small in the
 402 tropical free troposphere) and assuming that the boundary-layer temperature is tightly coupled to
 403 SST via turbulent surface heat fluxes, from (12) and the ideal gas law we expect the meridional
 404 wind to be proportional to the meridional SST gradient: $[v] \propto \partial SST / \partial \phi$. Neglecting gradients
 405 in $C/(f^2 + C^2)$, it follows that the low-level convergence and vertical velocity at the top of the
 406 boundary layer are proportional to the Laplacian (or curvature) of SST:

$$\omega_{BL} \propto \frac{\partial^2 SST}{\partial \phi^2}. \quad (13)$$

407 If the relationship (13) holds, it suggests that the ITCZ-edge latitude should scale with the latitude
 408 where the Laplacian of SST is zero.

409 In the idealized-GCM simulations, there is reasonable agreement between the simulated ITCZ-
 410 edge latitudes and the latitudes where $\partial^2 SST / \partial \phi^2 = 0$ (Figure 11a), with a correlation coefficient
 411 of $r = 0.89$. The ITCZ-edge estimates from this adapted Lindzen-Nigam theory do not lie on
 412 the one-to-one line, and there are several reasons for this. Most importantly we have assumed

413 Ekman balance which, as discussed, cannot fully capture ITCZ width across the simulations. We
414 have also assumed zero horizontal pressure gradients above the boundary layer and ignored verti-
415 cal momentum transport, though these assumptions are not generally valid (Back and Bretherton
416 2009). Finally, we have neglected meridional gradients in the drag coefficient and Coriolis pa-
417 rameter. Nevertheless, the prediction from Lindzen-Nigam theory that the ITCZ-edge latitude
418 should scale with the latitude where the Laplacian of SST is zero is found to approximately hold
419 in idealized-GCM simulations and provides a simple framework for understanding ITCZ-width
420 changes in response to changing SST patterns.

421 *b. Emanuel (1995) theory*

422 A complementary but distinct relationship between ITCZ width and surface temperature (and
423 humidity) can be derived following Emanuel (1995). Emanuel considered the transition between
424 an atmosphere in radiative-convective equilibrium (RCE) and an atmosphere with a thermally-
425 direct overturning circulation. He found that a sufficient condition for the RCE state to breakdown
426 and a circulation to emerge is for the meridional gradient in sub-cloud moist entropy to exceed a
427 critical threshold. Beyond this critical threshold, thermal wind becomes inconsistent with Hide's
428 theorem (Hide 1969) and a circulation spins up so as to reduce the meridional moist entropy
429 gradient. Assuming active convection and moist adiabatic lapse rates, Emanuel derived an expres-
430 sion for this critical moist entropy gradient and further argued that tropical surface winds can be
431 estimated by the degree to which the actual moist entropy distribution departs from the critical gra-
432 dient. Shaw and Voigt (2016) applied this theory to understand shifts in the Hadley circulation and
433 storm tracks under climate change, but it has not been applied to ITCZ width to our knowledge.

434 The Emanuel (1995) estimate for the balanced surface zonal wind is:

$$u_{\text{sfc}} = \frac{SST - T_t}{fa} \frac{\partial}{\partial \phi} (s - s_{\text{crit}}), \quad (14)$$

435 where T_t is the tropopause temperature (which we take to be the temperature at the $\sigma = 0.22$ level),
 436 $s = c_p \log \theta_e$ is the boundary-layer moist entropy, θ_e is the boundary-layer equivalent potential
 437 temperature and s_{crit} is the critical moist entropy distribution [see equation (7) of Shaw and Voigt
 438 (2016)]. Assuming Ekman balance, that $\tau_{x,\text{sfc}} \propto u_{\text{sfc}}$ and $u_{\text{sfc}} \propto [u]$, and neglecting meridional
 439 gradients in $SST - T_t$ and the Coriolis parameter, we find:

$$\omega_{\text{BL}} \propto \frac{\partial^2}{\partial \phi^2} (s - s_{\text{crit}}). \quad (15)$$

440 Expressed in words, (15) suggests that the ITCZ width scales with the latitude where the Laplacian
 441 of the departure of moist entropy from its critical distribution is zero. This scaling holds to some
 442 extent in the idealized-GCM simulations when an outlier is excluded (Figure 11) suggesting that
 443 ITCZ width is dynamically coupled to surface temperature and specific humidity via atmospheric
 444 convection and angular-momentum constraints.

445 8. Summary

446 The dynamical processes controlling ITCZ width have been investigated using idealized sim-
 447 ulations together with the boundary-layer zonal momentum budget and various scalings. In the
 448 simulations, Ekman processes place a strong constraint on ITCZ width: The boundary layer is ap-
 449 proximately in Ekman balance (Figure 2a) and the Ekman component of vertical velocity is large
 450 at the ITCZ edge (Figure 8). Scalings for ITCZ width based on Ekman dynamics are useful for
 451 understanding the behavior of ITCZ width across simulations (Figures 3, 4, 5, 6 and 7). In partic-
 452 ular, ITCZ width defined in terms of the mid-tropospheric streamfunction scales with the latitude
 453 where the surface *relative* vorticity is zero and the latitude where the meridional gradient in zonal

454 wind stress is zero (Figures 3). However, the boundary-layer definition of ITCZ width does not
455 scale with the latitude of zero relative vorticity — understanding why different metrics of ITCZ
456 width do not generally scale with one another is a topic for future work.

457 Although the ITCZ edge scales with the latitude where the wind stress maximizes, the ITCZ
458 edge robustly lies equatorward of the stress maximum due to meridional variations in the Coriolis
459 parameter (Figures 3). An analytical Ekman scaling for the ITCZ-edge latitude (4) suggests that
460 ITCZ width is directly proportional to the magnitude of the wind stress and inversely proportional
461 to its meridional gradient. The link between wind-stress magnitude and ITCZ width is also found
462 in the idealized-GCM simulations (Figure 7). The control of Ekman dynamics on ITCZ width
463 is examined in more detail using a toy model of the atmospheric boundary layer (Figure 6). The
464 ITCZ-width responses to simple wind-stress perturbations reveal non-intuitive behavior: Adding a
465 constant westerly (easterly) wind stress widens (narrows) the ITCZ (Figure 6a,b,c). The size of the
466 change in ITCZ width depends not only on the magnitude of the stress perturbation but also on the
467 curvature of the reference stress profile. Multiplying a reference wind-stress profile by a constant
468 factor does not shift the ITCZ edge (Figure 6d,e,f) but subtle changes in the latitude at which the
469 wind stress maximizes lead to large shifts in the ITCZ edge (Figure 6g,h,i). Given that angular
470 momentum imparted by the surface to the atmosphere in the tropics is transported poleward and
471 ultimately returned to the solid Earth by the mid-latitude surface westerlies (e.g., Held 2000), it is
472 clear that the dynamics of ITCZ width are connected to atmospheric circulations at higher latitudes
473 (Watt-Meyer and Frierson 2019) and the problem is therefore inherently non-local.

474 Although Ekman processes are a primary influence on ITCZ width, a scaling which includes
475 horizontal and vertical momentum advection [see equation (9)] is needed to quantitatively capture
476 ITCZ width across the full range of idealized-GCM simulations (Figure 4). The magnitudes of
477 the advection terms in the zonal momentum budget are small (Figure 2) but it is the meridional

478 gradients of these terms that control vertical velocity and ITCZ width, and advection contributes
479 substantially to vertical velocity at the ITCZ edge (Figure 8). Therefore a full, prognostic theory
480 for ITCZ width requires not only a prediction for wind-stress changes but also for changes in
481 horizontal and vertical momentum advection [though helpfully these advection terms are strongly
482 correlated (Figure 9)].

483 Because of the fast timescales of atmospheric processes relative to the slow timescales on which
484 ocean temperatures evolve, there has been a long-standing interest in developing theories for trop-
485 ical circulation/precipitation given the SST distribution (e.g., Sobel 2007). Extending the Lindzen
486 and Nigam (1987) theory we find, given a range of assumptions, that ITCZ width scales with the
487 latitude at which the Laplacian of SST is zero (Figure 11). An alternative model of the tropical
488 circulation (Emanuel 1995) suggests that ITCZ width scales with the latitude where the Laplacian
489 of the departure of the boundary-layer moist entropy from a critical distribution is zero. Our exten-
490 sions to the Lindzen and Nigam (1987) and Emanuel (1995) theories have some skill in capturing
491 the behavior of ITCZ width across the idealized-GCM simulations.

492 The analyses and scalings presented here establish a dynamical framework with which to un-
493 derstand the processes determining ITCZ width. This dynamical framework complements recent
494 efforts to understand ITCZ width based on the atmospheric energy budget (Chou et al. 2009; Byrne
495 and Schneider 2016a; Harrop and Hartmann 2016; Dixit et al. 2018) and has the potential to be
496 more informative and predictive, given that surface convergence and the ITCZ are driven predom-
497 inantly by boundary-layer pressure gradients and dynamics rather than by thermodynamic effects
498 higher in the atmosphere (Lindzen and Nigam 1987; Sobel and Neelin 2006; Back and Bretherton
499 2009). Our investigations into the dynamics of ITCZ width also advance fundamental understand-
500 ing of the atmospheric circulation, and are likely to be useful for examining ITCZ biases in more

501 complex climate models, differences in ITCZ width over land vs ocean regions, and the past and
502 future evolution of tropical rainfall.

503 *Acknowledgments.* This project has received funding from the European Union’s Horizon 2020
504 research and innovation programme under the Marie Skłodowska-Curie grant agreement No
505 794063. We also acknowledge support from the Imperial College London Research Fellowship
506 Scheme and useful discussions with Arnaud Czaja, David Battisti, Kerry Emanuel and Marty
507 Singh. This work used JASMIN, the UK collaborative data analysis facility.

508 **References**

509 Back, L. E., and C. S. Bretherton, 2009: On the relationship between SST gradients, boundary
510 layer winds, and convergence over the tropical oceans. *J. Climate*, **22**, 4182–4196.

511 Battisti, D. S., E. S. Sarachik, and A. C. Hirst, 1999: A consistent model for the large-scale steady
512 surface atmospheric circulation in the tropics. *J. Climate*, **12**, 2956–2964.

513 Bischoff, T., and T. Schneider, 2014: Energetic constraints on the position of the intertropical
514 convergence zone. *J. Climate*, **27**, 4937–4951.

515 Bretherton, C. S., and A. H. Sobel, 2002: A simple model of a convectively coupled Walker
516 circulation using the weak temperature gradient approximation. *J. Climate*, **15**, 2907–2920.

517 Broccoli, A. J., K. A. Dahl, and R. J. Stouffer, 2006: Response of the ITCZ to Northern Hemi-
518 sphere cooling. *Geophys. Res. Lett.*, **33**.

519 Byrne, M. P., A. G. Pendergrass, A. D. Rapp, and K. R. Wodzicki, 2018: Response of the in-
520 tertropical convergence zone to climate change: Location, width, and strength. *Current Climate*
521 *Change Reports*, **4**, 355–370.

522 Byrne, M. P., and T. Schneider, 2016a: Energetic constraints on the width of the intertropical
523 convergence zone. *J. Climate*, **29**, 4709–4721.

524 Byrne, M. P., and T. Schneider, 2016b: Narrowing of the ITCZ in a warming climate: Physical
525 mechanisms. *Geophys. Res. Lett.*, **43**, 11,350–11,357.

526 Byrne, M. P., and T. Schneider, 2018: Atmospheric dynamics feedback: concept, simulations and
527 climate implications. *J. Climate*, **31**, 3249–3264.

528 Chiang, J. C. H., and A. R. Friedman, 2012: Extratropical cooling, interhemispheric thermal
529 gradients, and tropical climate change. *Annu. Rev. Earth Planet. Sci.*, **40**, 383–412.

530 Chou, C., and J. D. Neelin, 2004: Mechanisms of global warming impacts on regional tropical
531 precipitation. *J. Climate*, **17**, 2688–2701.

532 Chou, C., J. D. Neelin, C.-A. Chen, and J.-Y. Tu, 2009: Evaluating the “rich-get-richer” mecha-
533 nism in tropical precipitation change under global warming. *J. Climate*, **22**, 1982–2005.

534 Dixit, V., O. Geoffroy, and S. C. Sherwood, 2018: Control of ITCZ width by low-level radiative
535 heating from upper-level clouds in aquaplanet simulations. *Geophys. Res. Lett.*, **45**, 5788–5797.

536 Donohoe, A., J. Marshall, D. Ferreira, and D. McGee, 2013: The relationship between ITCZ
537 location and cross-equatorial atmospheric heat transport: From the seasonal cycle to the Last
538 Glacial Maximum. *J. Climate*, **26**, 3597–3618.

539 Donohoe, A., and A. Voigt, 2017: Why future shifts in tropical precipitation will likely be small:
540 The location of the tropical rain belt and the hemispheric contrast of energy input to the atmo-
541 sphere. *Climate Extremes: Patterns and Mechanisms*, **226**, 115–137.

542 Emanuel, K. A., 1995: On thermally direct circulations in moist atmospheres. *J. Atmos. Sci.*, **52**,
543 1529–1536.

- 544 Emanuel, K. A., 2019: Inferences from simple models of slow, convectively coupled processes. *J.*
545 *Atmos. Sci.*, **76**, 195–208.
- 546 Frierson, D. M. W., 2007: The dynamics of idealized convection schemes and their effect on the
547 zonally averaged tropical circulation. *J. Atmos. Sci.*, **64**, 1959–1976.
- 548 Frierson, D. M. W., I. M. Held, and P. Zurita-Gotor, 2006: A gray-radiation aquaplanet moist
549 GCM. Part I: Static stability and eddy scale. *J. Atmos. Sci.*, **63**, 2548–2566.
- 550 Frierson, D. M. W., and Coauthors, 2013: Contribution of ocean overturning circulation to tropical
551 rainfall peak in the Northern Hemisphere. *Nat. Geosci.*, **6**, 940–944.
- 552 Gonzalez, A. O., C. J. Slocum, R. K. Taft, and W. H. Schubert, 2016: Dynamics of the ITCZ
553 boundary layer. *J. Atmos. Sci.*, **73**, 1577–1592.
- 554 Harrop, B. E., and D. L. Hartmann, 2016: The role of cloud radiative heating in determining the
555 location of the ITCZ in aquaplanet simulations. *J. Climate*, **29**, 2741–2763.
- 556 Held, I. M., 2000: The general circulation of the atmosphere. Lecture notes from the Woods Hole
557 Geophysical Fluid Dynamics Program.
- 558 Held, I. M., 2001: The partitioning of the poleward energy transport between the tropical ocean
559 and atmosphere. *J. Atmos. Sci.*, **58**, 943–948.
- 560 Held, I. M., and A. Y. Hou, 1980: Nonlinear axially symmetric circulations in a nearly inviscid
561 atmosphere. *J. Atmos. Sci.*, **37**, 515–533.
- 562 Hide, R., 1969: Dynamics of the atmospheres of the major planets with an appendix on the viscous
563 boundary layer at the rigid bounding surface of an electrically-conducting rotating fluid in the
564 presence of a magnetic field. *J. Atmos. Sci.*, **26**, 841–853.

- 565 Holton, J. R., 1975: On the influence of boundary layer friction on mixed rossby-gravity waves.
566 *Tellus*, **27**, 107–115.
- 567 Kang, S. M., I. M. Held, D. M. W. Frierson, and M. Zhao, 2008: The response of the ITCZ to
568 extratropical thermal forcing: Idealized slab-ocean experiments with a GCM. *J. Climate*, **21**,
569 3521–3532.
- 570 Kang, S. M., Y. Shin, and S.-P. Xie, 2018: Extratropical forcing and tropical rainfall distribution:
571 energetics framework and ocean Ekman advection. *npj Climate and Atmospheric Science*, **1**,
572 doi:10.1038/s41612-017-0004-6.
- 573 Lindzen, R. S., and S. Nigam, 1987: On the role of sea surface temperature gradients in forcing
574 low-level winds and convergence in the tropics. *J. Atmos. Sci.*, **44**, 2418–2436.
- 575 O’Gorman, P. A., and T. Schneider, 2008: The hydrological cycle over a wide range of climates
576 simulated with an idealized GCM. *J. Climate*, **21**, 5797–5806.
- 577 Peixóto, J. P., and A. H. Oort, 1984: Physics of Climate. *Reviews of Modern Physics*, **56**.
- 578 Philander, S. G. H., D. Gu, G. Lambert, T. Li, D. Halpern, N. C. Lau, and R. C. Pacanowski, 1996:
579 Why the ITCZ is mostly north of the equator. *J. Climate*, **9**, 2958–2972.
- 580 Popp, M., and L. G. Silvers, 2017: Double and single ITCZs with and without clouds. *J. Climate*,
581 **30**, 9147–9166.
- 582 Schneider, T., T. Bischoff, and G. H. Haug, 2014: Migrations and dynamics of the intertropical
583 convergence zone. *Nature*, **513**, 45–53.
- 584 Shaw, T. A., and A. Voigt, 2016: What can moist thermodynamics tell us about circulation shifts
585 in response to uniform warming? *Geophys. Res. Lett.*, **43**, 4566–4575.

- 586 Sobel, A. H., 2003: On the coexistence of an evaporation minimum and precipitation maximum
587 in the Warm Pool. *J. Climate*, **16**, 1003–1009.
- 588 Sobel, A. H., 2007: Simple models of ensemble-averaged precipitation and surface wind, given
589 the sea surface temperature. *The Global Circulation of the Atmosphere*, edited by T. Schneider
590 and A. H. Sobel, 219–251.
- 591 Sobel, A. H., and J. D. Neelin, 2006: The boundary layer contribution to intertropical conver-
592 gence zones in the quasi-equilibrium tropical circulation model framework. *Theor. Comput.*
593 *Fluid Dyn.*, **20**, 323–350.
- 594 Stevens, B., J. Duan, J. C. McWilliams, M. Münnich, and J. D. Neelin, 2002: Entrainment,
595 Rayleigh friction, and boundary layer winds over the tropical pacific. *J. Climate*, **15**, 30–44.
- 596 Su, H., and Coauthors, 2017: Tightening of tropical ascent and high clouds key to precipitation
597 change in a warmer climate. *Nat. Communications*, **8**, doi:10.1038/ncomms15771.
- 598 Taylor, K. E., R. J. Stouffer, and G. A. Meehl, 2012: An overview of CMIP5 and the experiment
599 design. *Bull. Amer. Meteor. Soc.*, **93**, 485–498.
- 600 Tomas, R. A., J. R. Holton, and P. J. Webster, 1999: The influence of cross-equatorial pressure
601 gradients on the location of near-equatorial convection. *Quart. J. Roy. Meteor. Soc.*, **125**, 1107–
602 1127.
- 603 Tomas, R. A., and P. J. Webster, 1997: The role of inertial instability in determining the location
604 and strength of near-equatorial convection. *Quart. J. Roy. Meteor. Soc.*, **123**, 1445–1482.
- 605 Waliser, D. E., and C. Gautier, 1993: A satellite-derived climatology of the ITCZ. *J. Climate*, **6**,
606 2162–2174.

- 607 Waliser, D. E., and R. C. J. Somerville, 1994: Preferred latitudes of the intertropical convergence
608 zone. *J. Atmos. Sci.*, **51**, 1619–1639.
- 609 Watt-Meyer, O., and D. M. W. Frierson, 2019: ITCZ width controls on Hadley cell ex-
610 tent and eddy-driven jet position, and their response to warming. *J. Climate*, doi:10.1175/
611 JCLI-D-18-0434.1, in press.
- 612 Wodzicki, K. R., and A. D. Rapp, 2016: Long-term characterization of the Pacific ITCZ using
613 TRMM, GPCP, and ERA-Interim. *J. Geophys. Res.: Atmos.*, **121**, 3153–3170.

614
615
616
617
618
619
620

621
622
623
624
625
626

627
628
629
630
631
632
633

634
635
636
637
638
639
640
641
642

643
644
645

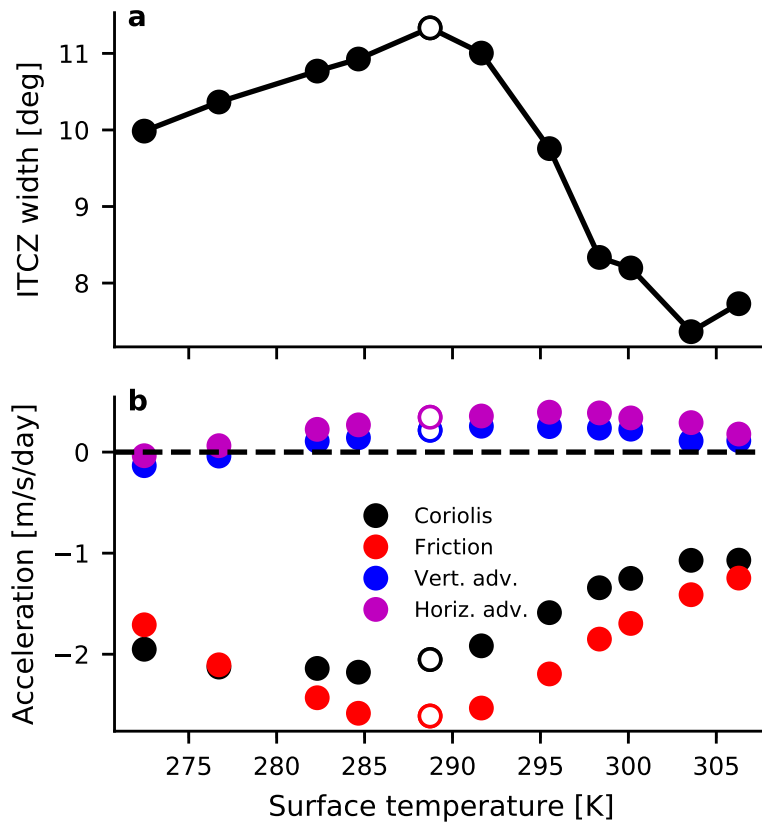
646
647
648
649
650
651
652
653
654
655

656
657

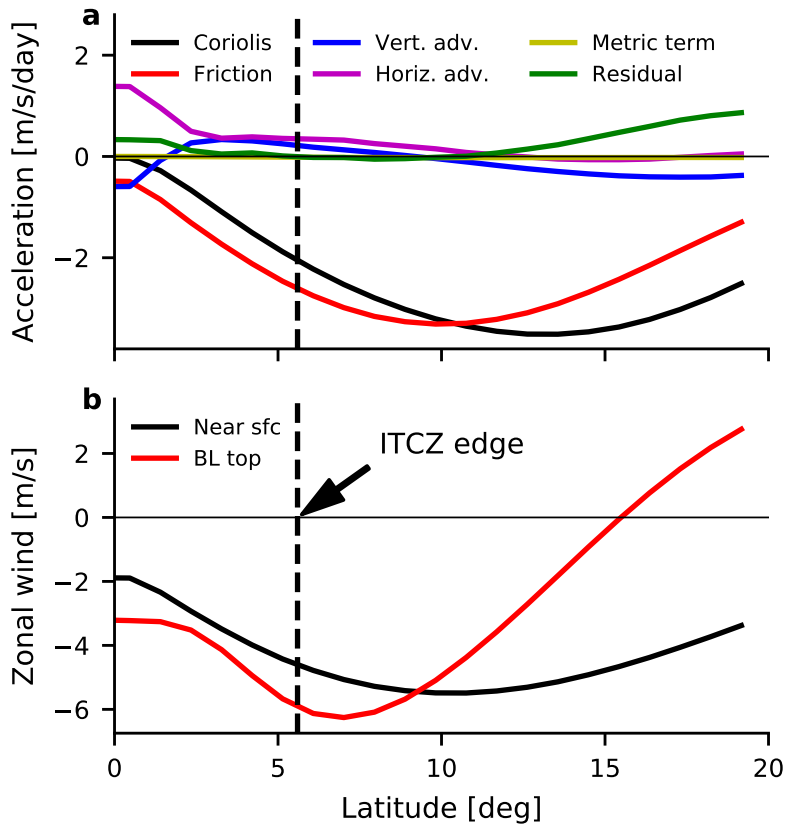
LIST OF FIGURES

- Fig. 1.** (a) ITCZ width and (b) the various terms in the boundary-layer zonal momentum budget (2) evaluated at the northern ITCZ edge vs global-mean surface temperature for the idealized-GCM simulations with different longwave optical thicknesses. The ITCZ edges are defined as the latitudes closest to the equator (north and south) where the vertical velocity at the top of the boundary layer is zero. Here and in subsequent figures unfilled circles denote the reference simulation with a scaling factor of $\alpha = 1.0$ for the longwave optical thickness. 34
- Fig. 2.** (a) Terms in the boundary-layer zonal momentum budget (2) for the reference simulation ($\alpha = 1.0$). The solid black line is the Coriolis term, the red line is the friction term, blue is the vertical advection term, magenta is the horizontal advection term, yellow is the metric term and green is the budget residual. (b) Near-surface zonal wind ($\sigma = 0.98$; solid black line) and zonal wind at the boundary-layer top ($\sigma = 0.8$). For panels (a) and (b), the vertical dashed black lines indicate the northern edge of the ITCZ. 35
- Fig. 3.** Northern latitudes of the ITCZ edges in the idealized-GCM simulations vs the ITCZ edges estimated as the latitudes where $\partial u_{\text{sfc}}/\partial \phi = 0$ (circles) and the latitudes where $\partial \tau_{x,\text{sfc}}/\partial \phi = 0$ (stars). For the simulated ITCZ edges (y-axis), black markers show the edges defined in terms of vertical velocity at the top of the boundary layer and red markers show the edges defined using an alternative definition based on the mid-tropospheric streamfunction. Specifically, the streamfunction definition calculates the ITCZ edges as the latitudes north and south of the equator at which the streamfunction maximizes. 36
- Fig. 4.** Northern latitudes of the ITCZ edges vs estimates of these latitudes using scalings (4) and (9). The black circles indicate the full scaling (9) and the red circles show the estimates assuming Ekman balance (4), i.e. excluding horizontal and vertical momentum advection. The blue circles show estimates from the full scaling (9) but including only the time-mean contributions to the advection terms (excluding the transient-eddy contributions). The transient-eddy contributions to momentum advection are estimated using 6-hourly model data. Smoothing is applied to the meridional gradients of the wind-stress and advection terms prior to evaluating the scalings. Here and in subsequent figures, the blue line indicates a one-to-one relationship. 37
- Fig. 5.** As in Figure 4 but here showing the simulated and estimated latitudes of the northern ITCZ edges in CMIP5 simulations. The pluses, crosses and triangles indicate the *aquaControl*, *aqua4K* and *aqua4xCO2* simulations, respectively. 38
- Fig. 6.** (a,d,g) Zonal wind stress, (b,e,h) meridional wind in the boundary layer and (c,f,i) vertical velocity at the top of the boundary layer in a toy Ekman model of the tropical atmosphere. The solid black lines denote the reference wind stress, meridional wind and vertical velocity profiles. In each column different perturbations have been applied to the reference stress profile: In panels (a,b,c) a constant westerly stress has been added (red lines) and subtracted (blue lines), in panels (d,e,f) the reference stress has been multiplied (red lines) and divided (blue lines) by a factor 2, and in panels (g,h,i) the latitude of maximum stress has been shifted equatorward (red lines) and poleward (blues lines). The colored circles show the latitudes of the ITCZ edges for the corresponding stress profiles, where the ITCZ edge is defined as the latitude at which the vertical velocity at the top of the boundary layer is zero. 39
- Fig. 7.** Latitude of the northern edge of the ITCZ vs the zonal wind stress at the ITCZ edge in the idealized-GCM simulations. 40

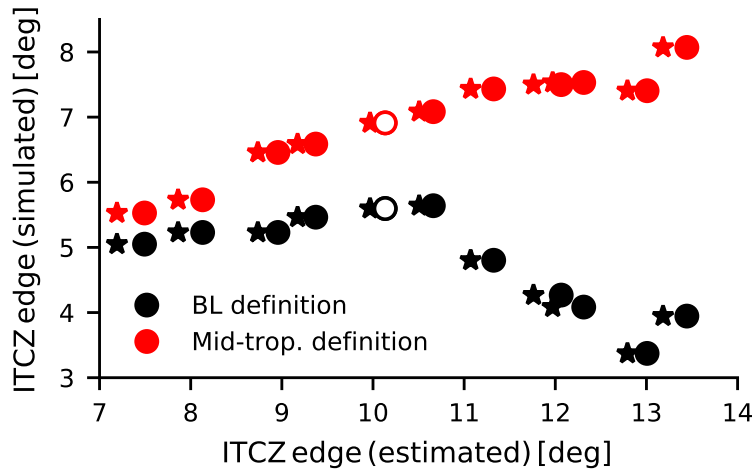
658	Fig. 8.	Vertical velocity at the top of the boundary layer ($\sigma = 0.8$) for the reference simulation (solid black line). Also shown are the Ekman (red line), vertical-advection (blue line), and horizontal-advection (magenta line) components of the vertical velocity as defined by (8), along with their sum (dashed-dotted black line). The dotted black line shows an estimate of vertical velocity for which meridional gradients in the reciprocal of the Coriolis parameter have been neglected. The vertical dashed black line indicates the northern ITCZ edge. Note that the hatched region close to the equator does not show the estimated vertical-velocity components; at these latitudes the $1/f \sim 1/\phi$ dependence causes each component to rapidly increase in magnitude as $\phi \rightarrow 0$	41
669	Fig. 9.	Horizontal vs vertical momentum advection terms in the zonal momentum budget (2), evaluated at the ITCZ edge for each idealized-GCM simulation.	42
670	Fig. 10.	Components of vertical velocity at the top of the boundary layer ($\sigma = 0.8$) at the ITCZ edge vs global-mean surface temperature for the idealized-GCM simulations.	43
671	Fig. 11.	Northern ITCZ edges in the idealized-GCM simulations vs the edges estimated as the latitudes closest to the equator where (a) the Laplacian of SST is zero and (b) the Laplacian of the departure of the simulated surface moist entropy distribution from the critical distribution is zero. See equations (13) and (15) for details. The correlation coefficients are $r = 0.89$ and $r = 0.21$ for panels (a) and (b), respectively. The correlation coefficient for (b) increases to $r = 0.77$ when the outlier is excluded.	44



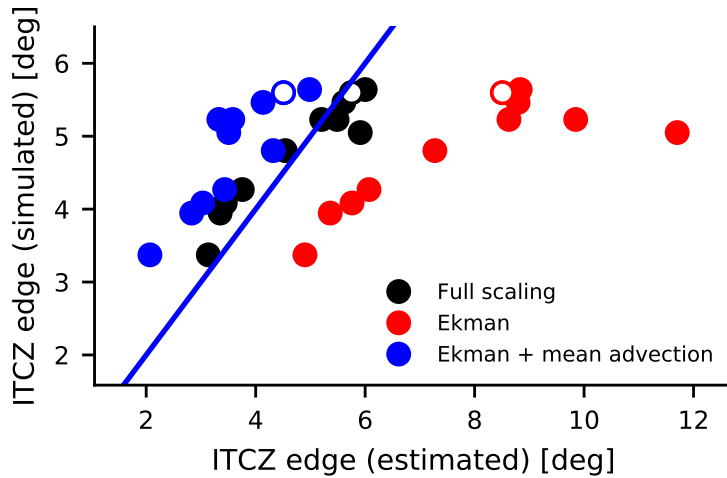
677 FIG. 1. (a) ITCZ width and (b) the various terms in the boundary-layer zonal momentum budget (2) evaluated
 678 at the northern ITCZ edge vs global-mean surface temperature for the idealized-GCM simulations with different
 679 longwave optical thicknesses. The ITCZ edges are defined as the latitudes closest to the equator (north and south)
 680 where the vertical velocity at the top of the boundary layer is zero. Here and in subsequent figures unfilled circles
 681 denote the reference simulation with a scaling factor of $\alpha = 1.0$ for the longwave optical thickness.



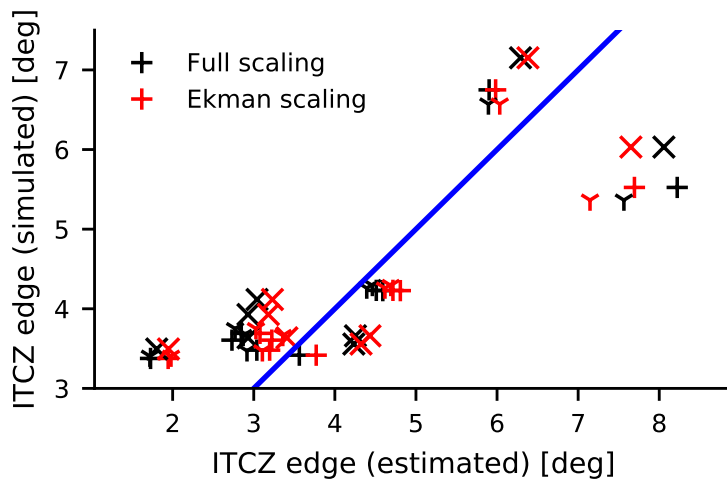
682 FIG. 2. (a) Terms in the boundary-layer zonal momentum budget (2) for the reference simulation ($\alpha = 1.0$).
 683 The solid black line is the Coriolis term, the red line is the friction term, blue is the vertical advection term,
 684 magenta is the horizontal advection term, yellow is the metric term and green is the budget residual. (b) Near-
 685 surface zonal wind ($\sigma = 0.98$; solid black line) and zonal wind at the boundary-layer top ($\sigma = 0.8$). For panels
 686 (a) and (b), the vertical dashed black lines indicate the northern edge of the ITCZ.



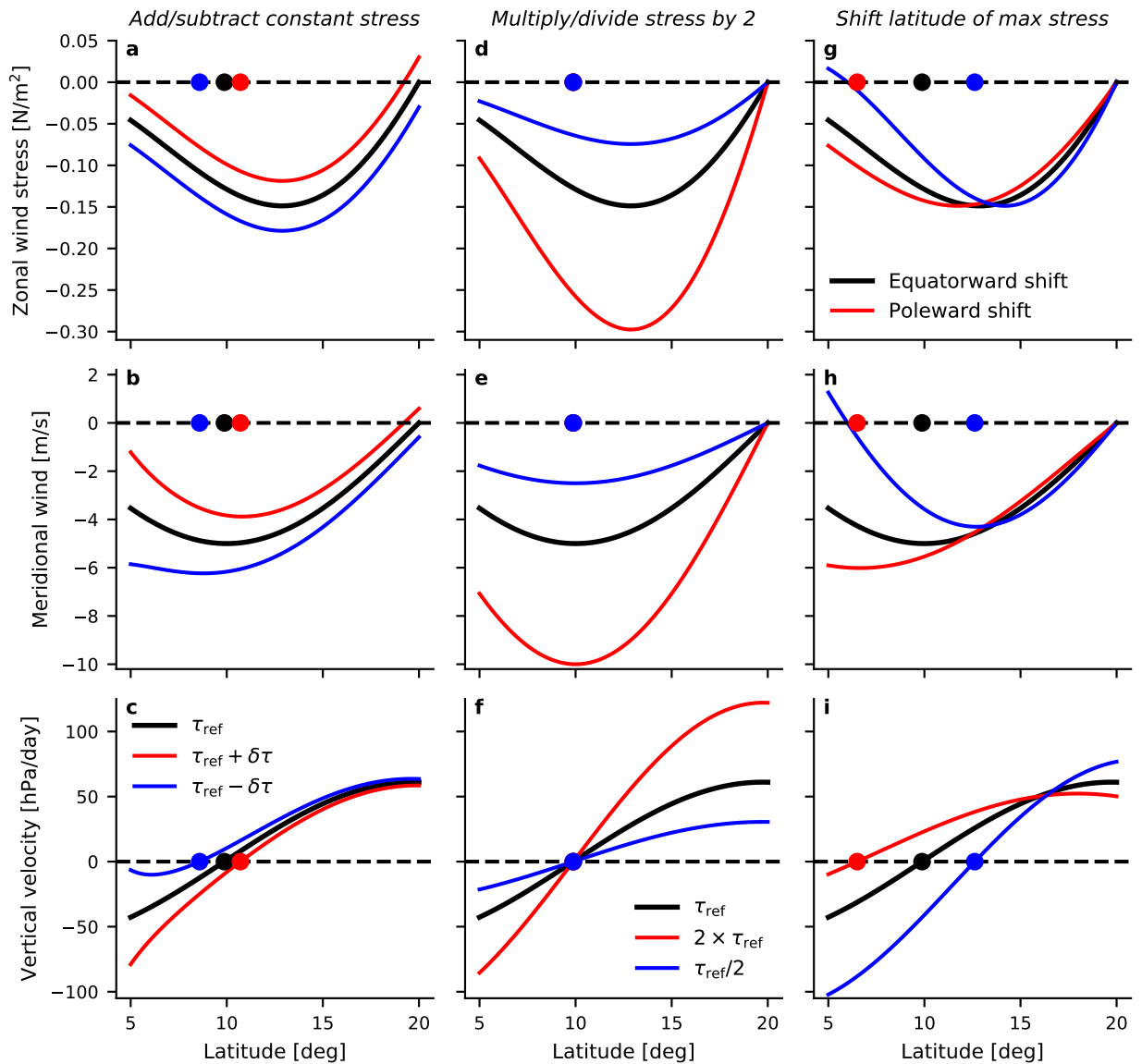
687 FIG. 3. Northern latitudes of the ITCZ edges in the idealized-GCM simulations vs the ITCZ edges estimated
 688 as the latitudes where $\partial u_{\text{sfc}}/\partial\phi = 0$ (circles) and the latitudes where $\partial\tau_{x,\text{sfc}}/\partial\phi = 0$ (stars). For the simulated
 689 ITCZ edges (y-axis), black markers show the edges defined in terms of vertical velocity at the top of the boundary
 690 layer and red markers show the edges defined using an alternative definition based on the mid-tropospheric
 691 streamfunction. Specifically, the streamfunction definition calculates the ITCZ edges as the latitudes north and
 692 south of the equator at which the streamfunction maximizes.



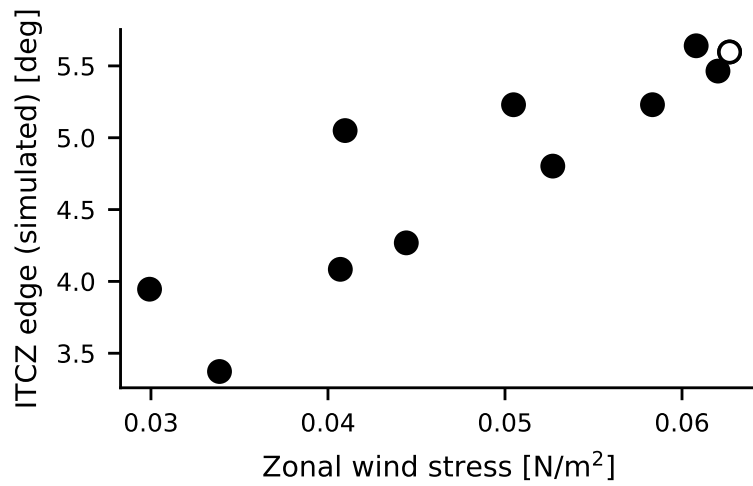
693 FIG. 4. Northern latitudes of the ITCZ edges vs estimates of these latitudes using scalings (4) and (9). The
 694 black circles indicate the full scaling (9) and the red circles show the estimates assuming Ekman balance (4),
 695 i.e. excluding horizontal and vertical momentum advection. The blue circles show estimates from the full
 696 scaling (9) but including only the time-mean contributions to the advection terms (excluding the transient-eddy
 697 contributions). The transient-eddy contributions to momentum advection are estimated using 6-hourly model
 698 data. Smoothing is applied to the meridional gradients of the wind-stress and advection terms prior to evaluating
 699 the scalings. Here and in subsequent figures, the blue line indicates a one-to-one relationship.



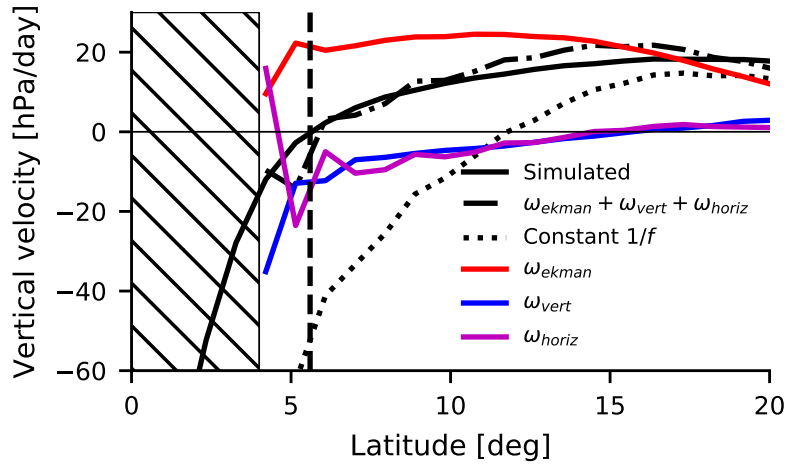
700 FIG. 5. As in Figure 4 but here showing the simulated and estimated latitudes of the northern ITCZ edges
 701 in CMIP5 simulations. The pluses, crosses and triangles indicate the *aquaControl*, *aqua4K* and *aqua4xCO2*
 702 simulations, respectively.



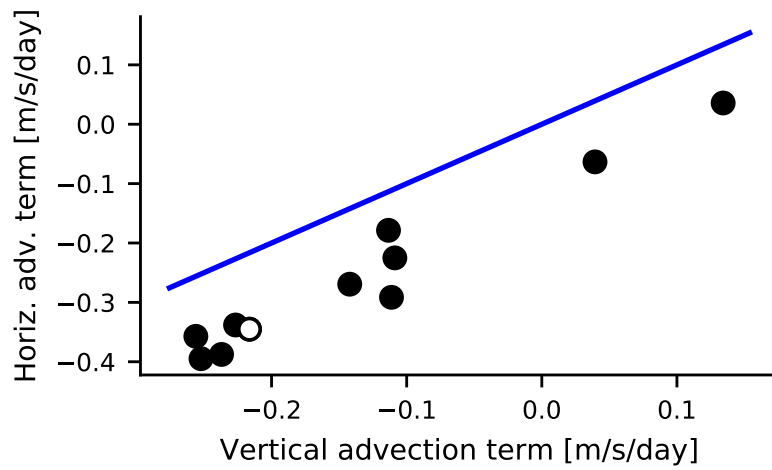
703 FIG. 6. (a,d,g) Zonal wind stress, (b,e,h) meridional wind in the boundary layer and (c,f,i) vertical velocity at
 704 the top of the boundary layer in a toy Ekman model of the tropical atmosphere. The solid black lines denote the
 705 reference wind stress, meridional wind and vertical velocity profiles. In each column different perturbations have
 706 been applied to the reference stress profile: In panels (a,b,c) a constant westerly stress has been added (red lines)
 707 and subtracted (blue lines), in panels (d,e,f) the reference stress has been multiplied (red lines) and divided (blue
 708 lines) by a factor 2, and in panels (g,h,i) the latitude of maximum stress has been shifted equatorward (red lines)
 709 and poleward (blue lines). The colored circles show the latitudes of the ITCZ edges for the corresponding stress
 710 profiles, where the ITCZ edge is defined as the latitude at which the vertical velocity at the top of the boundary
 711 layer is zero.



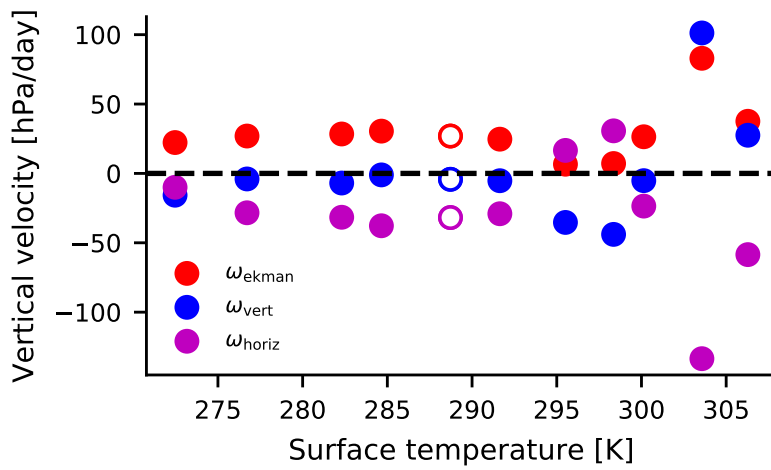
712 FIG. 7. Latitude of the northern edge of the ITCZ vs the zonal wind stress at the ITCZ edge in the idealized-
713 GCM simulations.



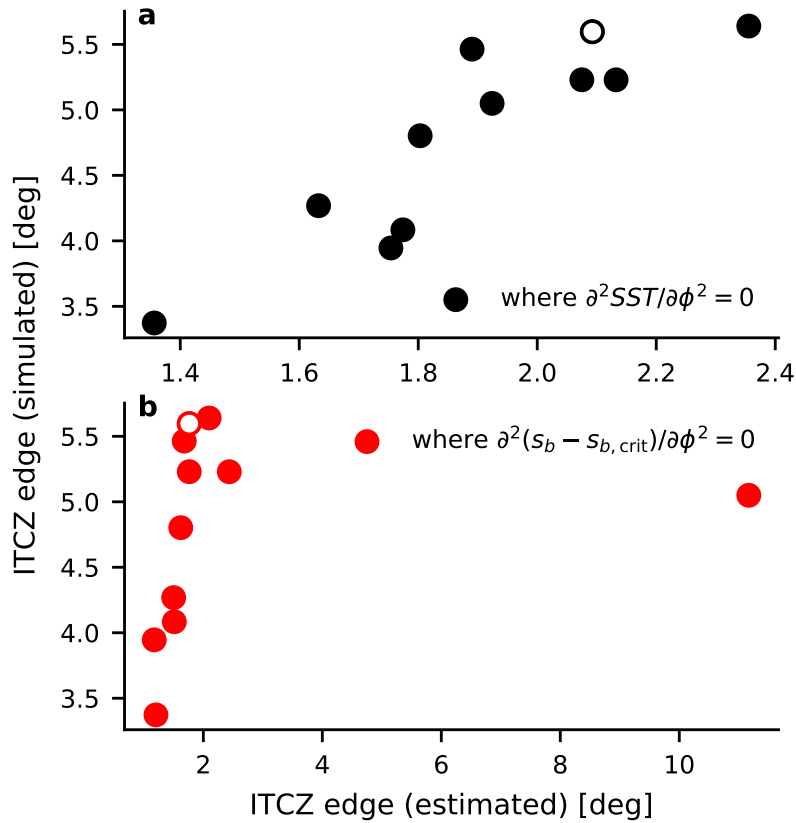
714 FIG. 8. Vertical velocity at the top of the boundary layer ($\sigma = 0.8$) for the reference simulation (solid black
 715 line). Also shown are the Ekman (red line), vertical-advection (blue line), and horizontal-advection (magenta
 716 line) components of the vertical velocity as defined by (8), along with their sum (dashed-dotted black line). The
 717 dotted black line shows an estimate of vertical velocity for which meridional gradients in the reciprocal of the
 718 Coriolis parameter have been neglected. The vertical dashed black line indicates the northern ITCZ edge. Note
 719 that the hatched region close to the equator does not show the estimated vertical-velocity components; at these
 720 latitudes the $1/f \sim 1/\phi$ dependence causes each component to rapidly increase in magnitude as $\phi \rightarrow 0$.



721 FIG. 9. Horizontal vs vertical momentum advection terms in the zonal momentum budget (2), evaluated at
 722 the ITCZ edge for each idealized-GCM simulation.



723 FIG. 10. Components of vertical velocity at the top of the boundary layer ($\sigma = 0.8$) at the ITCZ edge vs
 724 global-mean surface temperature for the idealized-GCM simulations.



725 FIG. 11. Northern ITCZ edges in the idealized-GCM simulations vs the edges estimated as the latitudes
 726 closest to the equator where (a) the Laplacian of SST is zero and (b) the Laplacian of the departure of the
 727 simulated surface moist entropy distribution from the critical distribution is zero. See equations (13) and (15)
 728 for details. The correlation coefficients are $r = 0.89$ and $r = 0.21$ for panels (a) and (b), respectively. The
 729 correlation coefficient for (b) increases to $r = 0.77$ when the outlier is excluded.